RESEARCH ARTICLE | APRIL 12 2023

A bi-directional flow-energy harvester ⊘

Lingwei Zeng ; Fuwang Zhao ; Hanfeng Wang ; Zhaokun Wang ; Waikin Yeung ; Yang Liu ;
Hui Tang ✉

Check for updates

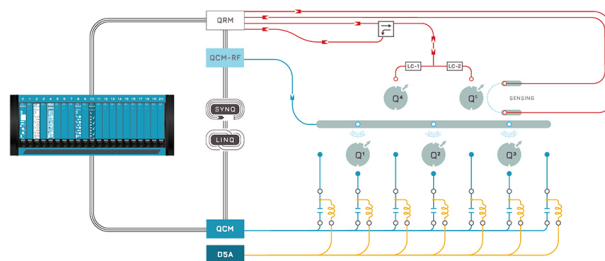View Online   Export Citation   CrossMark

A bi-directional flow-energy harvester

View Online   Export Citation   CrossMark

Lingwei Zeng,[1] (iD) Fuwang Zhao,[1] (iD) Hanfeng Wang,[2] (iD) Zhaokun Wang,[1] (iD) Waikin Yeung,[1] (iD) Yang Liu,[1] (iD)
and Hui Tang[1,a] (iD)

AFFILIATIONS

[1]Department of Mechanical Engineering, The Hong Kong Polytechnic University, Kowloon, Hong Kong, China
[2]School of Civil Engineering, Central South University, Changsha, Hunan 410075, China

[a]Author to whom correspondence should be addressed: h.tang@polyu.edu.hk

ABSTRACT

Due to a rapid decrease in fossil fuel resources and ever-growing carbon emissions, clean energy is urgently needed as a vital solution. In the past two decades, harvesting clean energy from ambient environment has attracted much attention. Flow induced vibration and energy harvesting performance of a cylinder with fins attached were investigated. Four configurations were studied: a plain cylinder, a cylinder with two windward fins, a cylinder with two leeward fins, and a cylinder with four fins. These four cylinders were tested in a water channel with a reduced velocity ranging between 2 and 25 and a Reynolds number ranging between 1500 and 11 400. It was found that the two-windward-fin cylinder underwent galloping, exhibiting much larger vibration amplitudes and a much broader operational velocity range, whereas the two-leeward-fin cylinder only underwent weak vortex-induced vibrations. By attaching both two windward and two leeward fins to the cylinder, a bi-directional flow-energy harvester was implemented, which outperformed the plain cylinder with much larger vibration amplitudes and a much broader velocity range. More importantly, due to the geometric symmetry, it is able to harvest flow energy from two opposite directions. A tuned-mass-damper system was then attached to the four-fin cylinder for the purpose of demonstration. Within the current flow speed range, the maximal voltage and power outputs are about 7.37 V and 1.81 μW, respectively, about 2.7 and 7.2 times the plain cylinder's peak values. The effects of flow incident angle and fin length were also studied. Numerical simulations were also conducted to provide a detailed information of flow and pressure to uncover the underlying physics. This bi-directional flow-energy harvester is a suitable candidate to operate at sites where the flow periodically switches its directions, such as in tidal flows.

Published under an exclusive license by AIP Publishing. https://doi.org/10.1063/5.0140569

Harvesting energy from environmental flows has been attracting much attention in recent years, which can play an important role for low-power electronics such as sensors in remote areas where cable connections are not always available or in condensed city areas where space is usually a constraint.[1–8] This type of flow-energy harvesting can be realized through three types of flow-induced vibration (FIV) of bluff bodies, including vortex-induced vibration (VIV), galloping, and flutter. An elastically supported circular or square cylinder is the most representative case.[9–15] To improve the performance, the use of appendages is one of the most effective methods. For example, Hu *et al.*[16] studied the performance of a circular cylinder appended with two parallel cylindrical rods. They reported that when the circumferential angle of the rod, θ, increased from 0° (the front stagnation point) to 60°, the system's vibration mode changed from VIV to galloping. However, when θ further increased to 90°, the vibration was almost suppressed. At $\theta = 60°$ and rods' diameter $d/D = 2.5\%$, the system achieved the maximum voltage (11 V) and power (24.2 μW) outputs, about 2.5 and 6.25 times higher than those

for the plain cylinder, respectively. Recently, Wang *et al.*[17] studied the energy harvesting performance of a circular cylinder using two fins. They also confirmed that the system obtained the best performance at $\theta = 60°$, and the vibration was almost fully suppressed at $\theta = 120°$.

The above studies suggested that adding attaching appendages on the windward side, especially at $\theta = 60°$, can promote the vibration and, hence, the energy harvesting performance of bluff bodies, while attaching appendages on the leeward side does the opposite. This implies that the appendages only perform well in one dominant flow direction. This unidirectional issue can be addressed by deploying appendages on both the windward and leeward sides, allowing bi-directional usage of the device. However, using a square cylinder, Hu *et al.*[18] revealed that this configuration can only achieve similar performance as the plain cylinder. In the present study, we demonstrated that deploying fins on both the windward and leeward sides can achieve a bi-directional flow-energy harvester with much larger energy output and much broader operational velocity range than the plain
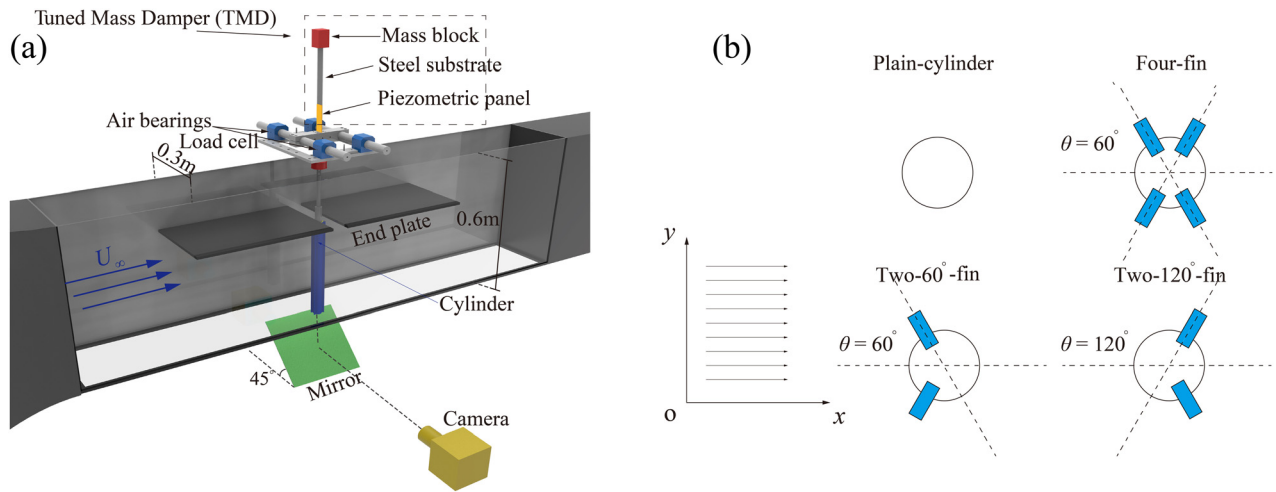
FIG. 1. Sketches of (a) the test rig and (b) the four cylinders used in the experiments, where the displacement was recorded by a high-speed camera, and the force was measured by a load cell.

cylinder. Furthermore, this concept also seems robust to flow disturbance in terms of both the speed and direction of the flow.

The experiments were carried out in a closed-loop water channel. As shown in Fig. 1(a), a circular cylinder of diameter $D = 22$ mm and length $L = 430$ mm was vertically placed at the center of the test section, resulting in a blockage ratio of 7.3%. The total mass of the cylinder and its supporting moving shaft was around $m = 9.8$ kg, corresponding to a mass ratio $m^* = 4m/\pi\rho D^2 L \approx 54$, where ρ is the water density. By carrying out free decay tests, the system's structural damping was determined as $\zeta_s = 0.6\%$, such that $m^*\zeta_s = 0.324$, and the natural frequency was determined as $f_n = 0.97$ Hz.

To convert the mechanical energy of the oscillating cylinder into electricity, a tuned-mass-damper (TMD) system was installed in line with the cylinder, which consists of a mass block vertically supported by a steel beam of 320 mm long, 25 mm wide, and 0.75 mm thick. A piezoelectric macro-fiber composite sheet (M8514P2) of 100 mm long, 14 mm wide, and 0.35 mm thick was attached to the root of the steel beam. Therefore, electric voltage can be generated by the piezoelectric sheet through the deformation of the steel beam. Four different configurations were considered: the plain cylinder (serving as the baseline case), the cylinder attached with two windward fins, with two leeward fins, and with four fins (i.e., two windward and two leeward), as sketched in Fig. 1(b). The test conditions for the four cylinders are listed in Table I. The incident angle was set as $\alpha = 0°$, and the fin

TABLE I. Summary of the test cases.

Cases	Reduced velocity (U_r)	Incident angle (α)	Length of fin (L/D)
Plain-cylinder	2–25	⋯	0
Four-fin	2–25	0°, 2.5°, 5°, 8°	0.25, 0.5
Two-leeward-fin	2–25	0°	0.25
Two-windward-fin	2–25	0°	0.25

length was set as $L = 0.25D$. As the proposed concept, the four-fin cylinder was also tested with three more different incident angles, i.e., $\alpha = 2.5°$, $5°$, and $8°$, and one more fin length, i.e., $L = 0.5D$.

Figure 2(a) presents the root mean square values of the dimensionless vibration displacement, y_{rms}, against the reduced velocity, U_r ($= U_\infty/f_n D$), for the four cylinders. The plain cylinder exhibits a typical VIV response with an initial branch in $3.7 < U_r \leq 5.3$, where y_{rms} rises sharply to reach a peak of $0.43D$, and a lower branch in $5.3 < U_r \leq 10.1$, where y_{rms} gradually decreases to a small value close to 0. This trend is consistent with what have been reported in the literature,[19–22] in which the systems have similar $m^*\zeta_s$ values.

The dynamics of the cylinder was drastically changed when fins were deployed. When two fins were deployed at the windward side, y_{rms} sharply increases once U_r exceeds a threshold of 5.35 and does not seem to reach its level off in the current U_r range, revealing great energy harvesting potentials. This is a typical galloping response, as having been reported in the literature.[19,23–25] However, when the two fins were deployed at the leeward side, the cylinder's oscillation was almost fully suppressed. The huge difference between these two cases suggests that, although very promising, the energy harvesting system with two fins attached at the windward side is only unidirectional. As a trade-off between these two extreme cases, the four-fin case experienced intermediate oscillations in a broad U_r range, showing a mild galloping response. This observation is similar to those reported in Refs. 16 and 17. Due to the symmetric arrangement of the four fins, it is very suitable to extract energy from tidal flows or onshore/offshore winds where the flow direction usually switches between two opposite directions.

For the four-fin cylinder, Fig. 2(b) further shows the effects of α, the incident angle, and L/D, the fin length, on y_{rms}. It is seen that when α is relatively small, i.e., $\alpha = 0°$ and $2.5°$, the system exhibits gallop-type dynamics, while when α is relatively large, i.e., $\alpha = 8°$, the system exhibits VIV-type dynamics. At the intermediate $\alpha = 5°$, the VIV-gallop hybrid dynamics is observed. That is, y_{rms} gradually drops after reaching its peak, and increases again at large U_r. In general, y_{rms} reduces with α, especially at large U_r. These observations suggest that
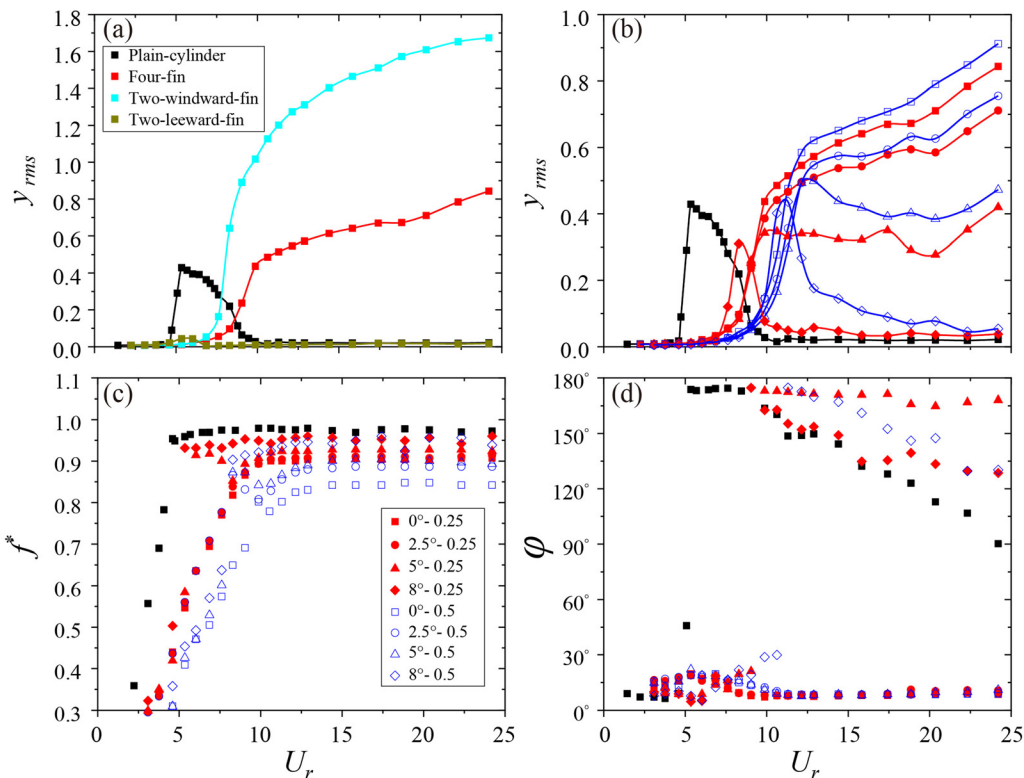
FIG. 2. Dynamic response comparison: (a) y_{rms} of the four typical cases; (b), (c), and (d) y_{rms}, dimensionless frequency f^*, and phase angle φ of the four-fin case with different α and L/D.

the current system is robust in flow-energy harvesting when the incoming flow deviates from the designed direction within $\pm 5°$, but its performance deteriorates at larger incident angles.

It is also seen from Fig. 2(b) that the increase in L/D from 0.25 to 0.5 can generally increase y_{rms}, especially at relatively small α. This is consistent with what has been reported in Ref. 16, where this increasing trend was observed in a smaller fin length range, i.e., from 0.025 to 0.2, at $\alpha = 0°$. At the larger incident angle, i.e., $\alpha = 8°$, the y_{rms}–U_r responses become the VIV type. In this scenario, the increase in L/D not only enhances the y_{rms} peak but also pushes the onset of the y_{rms} peak to larger U_r values, which is not surprising since the attachment of the four fins increases the effective diameter of the cylinder.

The change of the incident angle and fin length also changes the system's other dynamic characteristics, such as the vibration frequency and the force–displacement phase angle. As shown in Fig. 2(c), the plain cylinder's vibration frequency $f^* = f/f_n$, where f is the cylinder's dominant oscillation frequency, is locked around unity regardless of U_r. This is attributed to the large inertia ($m^* = 54$) adopted in the current system, such that the system's frequency is dominated by its own inertia and stiffness, rather than the excitation of the fluid force. When the four fins are attached with zero incident angle, the dominant vibration frequency reduces to $f^* \approx 0.90$ for the $L/D = 0.25$ case and $f^* \approx 0.85$ for the $L/D = 0.5$ case, regardless of U_r. This is probably caused by the increased added mass brought by the fins. As α increases, the vibration frequency gradually increases toward unity,

reflecting the reduction of added mass when the deviation of incident angle breaks the symmetry of the fins on the cylinder.

The variations of force–displacement phase angle φ are compared in Fig. 2(d). Here, φ is evaluated as $\varphi = \arccos R(C_y, y)$, where $R(C_y, y)$ is the correlation coefficient between the transverse hydrodynamic force C_y and the oscillation displacement y. For the plain cylinder, φ suddenly jumps from around $0°$ to about $180°$ at the onset of VIV ($U_r \approx 5.1$), reflecting the occurrence of lock-in phenomena. After the lower branch ($5.3 < U_r \leq 10.1$), φ gradually decreases to around $90°$. Similar trends are also observed for the $\alpha = 8°$ case, regardless of the fin length. For the $\alpha = 0°$ and $2.5°$ cases where galloping occurs, φ generally remains at low values, revealing the dominant fluid-to-structure energy flow in this type of FIV phenomenon. For the $\alpha = 5°$ cases, it is interesting to see φ jumps and then remains at unity in the $L/D = 0.25$ case, whereas φ remains at very low values in the $L/D = 0.5$ case. This observation confirms that the $\alpha = 5°$ configuration is near the VIV-gallop boundary.

To unveil the underlying physics associated with the change of dynamics for cylinders with different fin settings, simulations were conducted to show more details using ANSYS Fluent. The vortex structures and pressure fields around the four cylinders at selected instants in a half vibration period, from the top extreme to the bottom extreme, are presented in Figs. 3 and 4, respectively. For the plain cylinder oscillating with its maximum amplitude at $U_r = 5.3$, shear layers are alternatively formed and shed from the top and bottom sides of
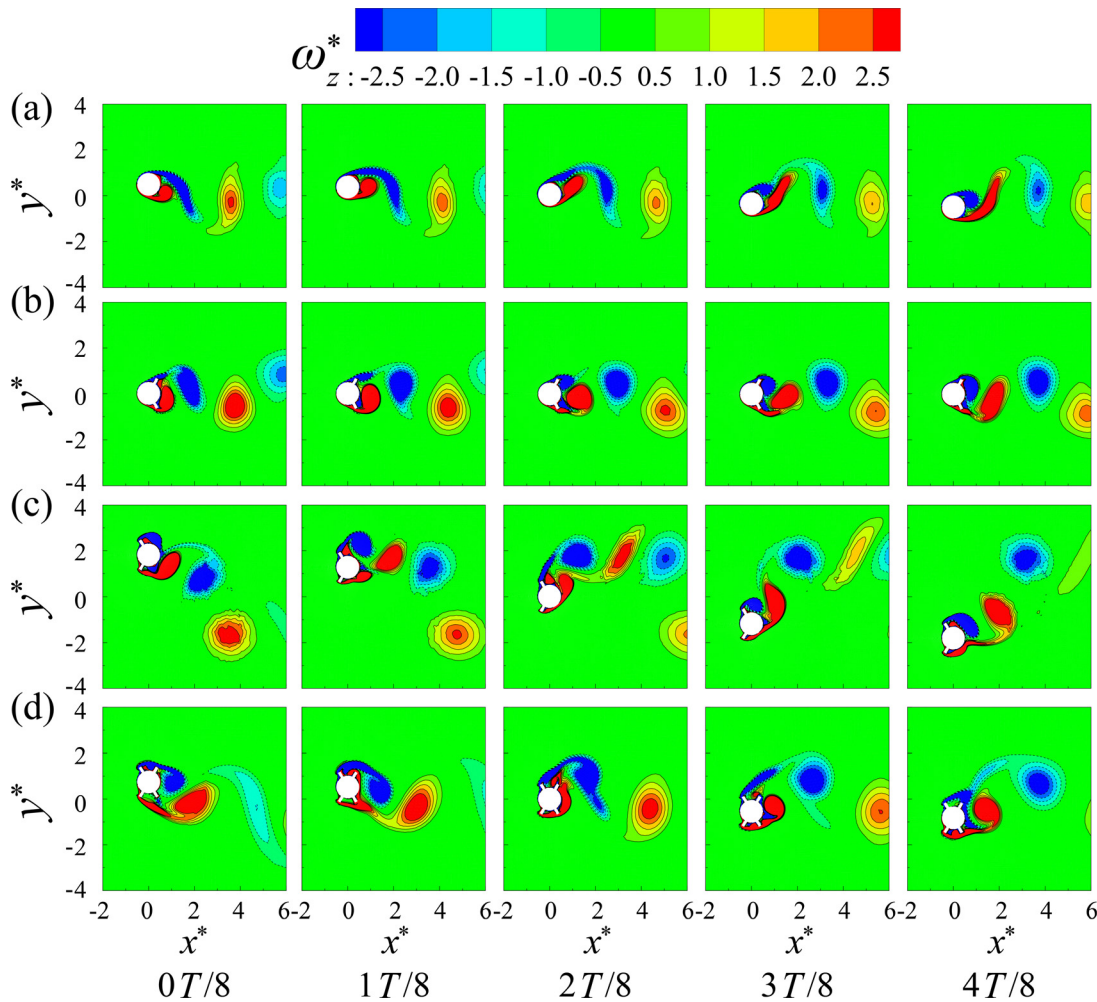
FIG. 3. Instantaneous vortex patterns around (a) plain cylinder, $U_r = 5.3$; (b) two-windward-fin cylinder, $U_r = 10.0$; (c) two-leeward-fin cylinder, $U_r = 10.0$; and (d) four-fin cylinder, $U_r = 10.0$. $0T/8$, $2T/8$, and $4T8$ represent the instants when the cylinder is at the highest position, moving downward through the equilibrium position, and at the lowest position, respectively. ω_z^* is the spanwise vorticity normalized by D and U_∞.

the vibrating cylinder, generating a pair of vortices in one vibration period and forming the classical 2S vortex mode [Fig. 3(a)]. A corresponding low-pressure region emerges when the shear layer rolls up into a vortex, which is initiated from the top/bottom side of the cylinder and then gradually develops to the rear side, as shown in Fig. 4(a). These alternatively appearing low-pressure regions always force the cylinder to return to its equilibrium position (i.e., $y^* = 0$). That is, they accelerate the cylinder when it is moving toward the equilibrium position, and decelerate the cylinder when it is moving away. As such, two-way energy transfer occurs between the flow and the cylinder system.

For the cylinder attached with two leeward fins operating at $U_r = 10.0$, the room left for the development of shear layers is limited by the fins. Instead of separating from the cylinder surface, these shear layers are first pushed away by the two fins and then forced to separate at the fin tips, forming larger and stronger vortex pairs in the wake [see Fig. 3(b)]. The associated low-pressure regions, although very

strong, are then mainly further downstream the two fins, more on the back side of the cylinder [Fig. 4(b)]. As such, the cylinder experiences much less net vertical force compared to the plain cylinder. This explains why the two-leeward-fin cylinder exhibits the least vibration among all four cases.

When the two fins are installed on the windward side, flow separation is early promoted at the fin tips. The separated shear layer on the bottom side quickly re-attaches on the cylinder's downstream convex surface, and is further elongated and bent by the cylinder's downward motion, as revealed at instant $2T/8$ in Fig. 3(c). The bent of the shear layer generates a very strong low-pressure region right on the cylinder's bottom side, as shown in Fig. 4(c), producing a very large net vertical force. This net vertical force seems nearly in phase with the cylinder's displacement [consistent with the observation in Fig. 2(d)], and, hence, results in a much larger vibration amplitude, as shown in Fig. 2(a). That is, the cylinder is undergoing galloping.
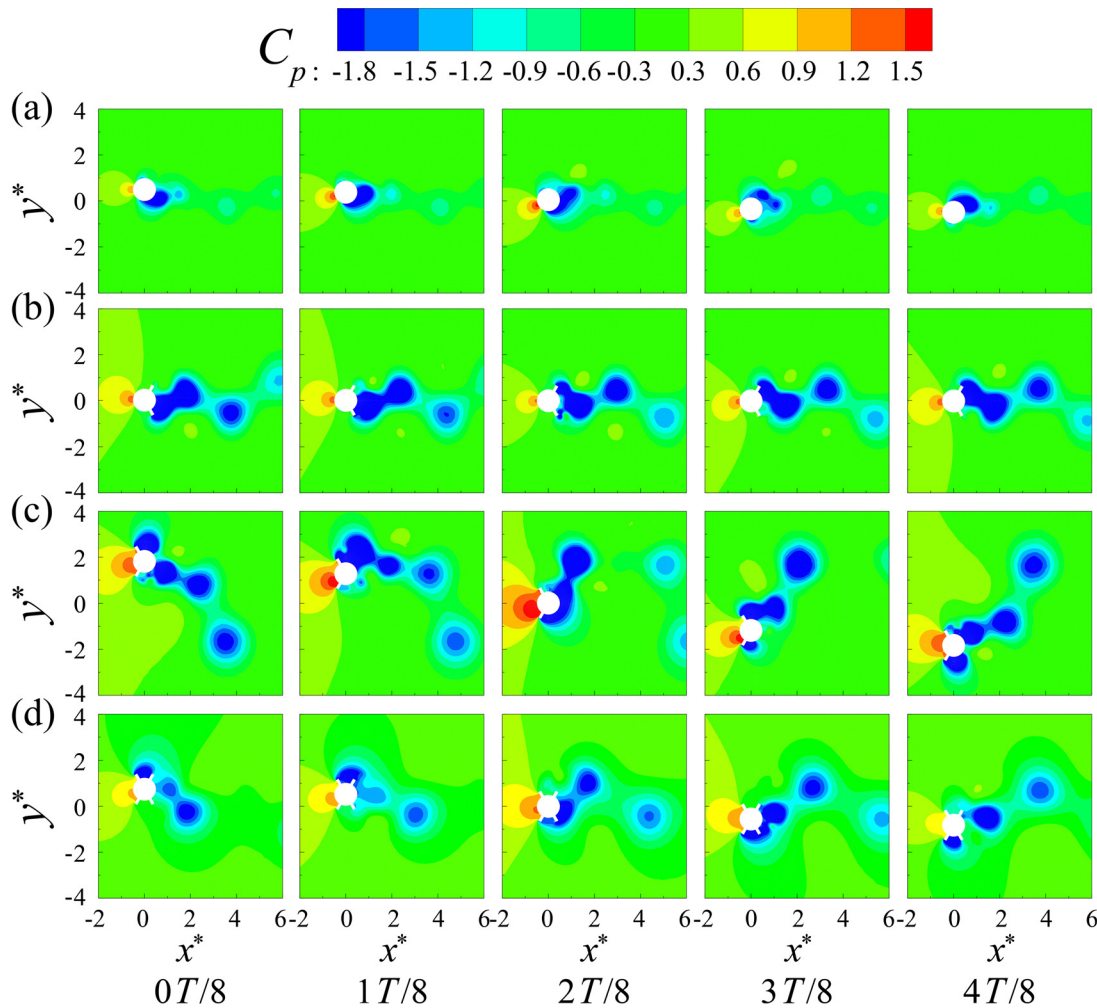
FIG. 4. Instantaneous pressure field at typical cases: (a) plain-cylinder case, $U_r = 5.3$; (b) two-windward-fin case, $U_r = 10.0$; (c) two-leeward-fin case, $U_r = 10.0$; and (d) four-fin case, $U_r = 10.0$.

As for the four-fin cylinder, the two windward fins promote flow separation at the fin tips, while the two leeward fins force the re-attached shear layer, if any, to separate again, as shown in Fig. 3(d). Similar to the two-windward-fin cylinder case, a strong low-pressure region around the bottom side of the cylinder is formed due to the lower-side separated shear layer reattaching to the cylinder as it moves downward, as revealed at instant $2T/8$ in Fig. 4(d). The lower leeward fin disrupts this reattachment and mitigates further bending of the shear layer along the cylinder surface. As such, the low-pressure region is mainly confined between the windward and leeward fins and, hence, becomes smaller and weaker than in the two-windward-fin cylinder case. This generates reduced pressure imbalance in the vertical direction, resulting in mild y_{rms} [Fig. 2(a)].

The output voltage depends on the load resistance deployed in the piezoelectric circuit. A simple test revealed that, at a selected wind speed $U_r = 14.5$, the output voltage V_{rms} reaches its maximum value 5.85 V when the load resistance $R = 30$ MΩ. Therefore, we adopted this load resistance to compare the energy harvesting performance of

the four-fin cylinder cases. Figure 5(b) presents the generated voltage V_{rms} with different fin length L/D and incident angle α. The maximum V_{rms} value (7.37 V) appears in the $\alpha = 0°$ and $L/D = 0.25$ case, which is about 2.7 times the peak voltage in the plain cylinder case. The voltage trends seem similar to the A_{rms} trends shown in Fig. 2(b). That is, the $\alpha = 0°$ and $2.5°$ cases show monotonically increasing V_{rms} against U_r, whereas the $\alpha = 8°$ and $L/D = 0.25$ case shows a similar variation trend as that for the plain cylinder. Differences are also observed. First, the $L/D = 0.5$ cases may not always perform better than the $L/D = 0.25$ cases, e.g., the two $\alpha = 0°$ cases. Second, the $\alpha = 5°$ and $L/D = 0.25$ case exhibits the VIV type response, instead of the VIV-gallop hybrid response in its vibration amplitude. Third, the $\alpha = 8°$ and $L/D = 0.5$ case exhibits the VIV-gallop hybrid response instead of the VIV type response in its vibration amplitude. All these changes can be attributed to the attachment of the TMD system to the cylinder, which, although less dominant, makes dynamics of the integrated system slightly different from the dynamics of pure cylinder system.
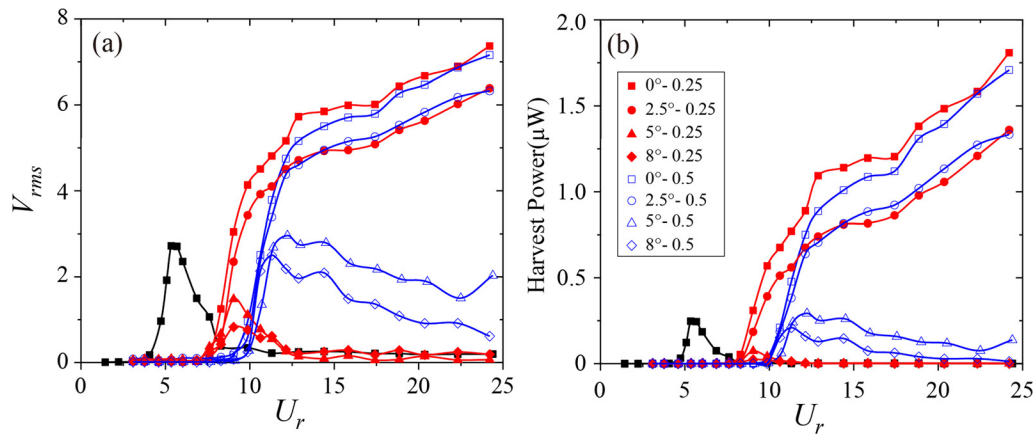
FIG. 5. (a) and (b) Variation of V_{rms}, P_{avg} for the four-fin case with different α and L/D.

Figure 5(c) further compares the mean power (defined as $P_{avg} = V_{rms}^2/R$) among the four-fin cases. The overall trends for P_{avg} are similar to those for V_{rms}. Compared with the plain cylinder case, the maximum P_{avg} appearing in the $\alpha = 0°$ and $L/D = 0.25$ case at $U_r = 24.2$ is about 1.81 μW, about 7.2 times the peak power in the plain cylinder case. The output power density is defined as $P_d = P_{avg}/V_P$, and V_P is the volume of the piezoelectric sheets.[26] P_d for our plain-cylinder case is about 0.51 mW/cm^3 (at $U = 0.11$ m/s), smaller than that reported by Sun et al.[27] ($P_d = 1.949$ mW/cm^3 at $U = 0.48$ m/s), Wang et al.[17] ($P_d = 4.76$ mW/cm^3 at $U = 1.5$ m/s), and Hu et al.[16] ($P_d = 7.89$ mW/cm^3 at $U = 2.1$ m/s). This suggests that our setup is not optimized and has a large room for improvement. It is not surprising, because, in our case, the piezoelectric sheet was attached only at one end of the vibration, while in their cases, it was attached at both ends. In addition, this study is not focusing on optimizing the performance of the harvesters; we aim to conceptualize the higher performance of this bi-directional flow-energy harvester compared to the plain-cylinder case.

In summary, we proposed a flow-energy harvester by attaching four small fins on an elastically supported circular cylinder. Major findings are as follows:

(1) The four-fin cylinder combines the features of both the two-windward-fin and the two-leeward-fin cylinder designs. The combination of these four fins renders the cylinder with the capability of harvesting flow energy in a broad velocity range from two opposite directions. This great feature makes this concept suitable to operate at sites where the flow periodically switches between two opposite directions, such as in tidal flows.

(2) Compared to the plain cylinder, the four-fin cylinder is able to harvest much more flow energy in a much broader velocity range by promoting instead of suppressing galloping, although it requires a larger cut-in speed to operate. Within the current flow speed range, the maximum voltage and power outputs are about 7.37 V and 1.81 μW, respectively, about 2.7 and 7.2 times the peak values for the plain cylinder. Since the maximum tested speed in the present experiment is only about 0.5 m/s, the energy harvesting performance can be further improved at higher flow speeds.

(3) This concept is robust to flow disturbance in terms of both the speed and direction of flows. On the one hand, with a board operational velocity range, it can sustain in flows with speed fluctuations. On the other hand, it works well in flows whose direction slightly deviates from the prevailing direction (within $\pm$ 5°).

Although only demonstrated in the laboratory settings, the concept can be easily scaled up to operate in actual river and ocean flows. In addition, the concept can be arrayed in different configurations to form a farm, which will be investigated in our future studies.

AUTHOR DECLARATIONS
Conflict of Interest

The authors have no conflicts to disclose.

Author Contributions

Lingwei Zeng and Fuwang Zhao contributed equally to this work.

Lingwei Zeng: Data curation (equal); Formal analysis (equal); Investigation (equal); Methodology (equal); Software (equal); Writing – original draft (equal); Writing – review & editing (equal). **Fuwang Zhao:** Data curation (equal); Methodology (equal); Software (equal); Writing – original draft (equal). **Hanfeng Wang:** Supervision (equal); Writing – review & editing (equal). **Zhaokun Wang:** Methodology (equal); Software (equal). **Waikin Yeung:** Project administration (equal). **Yang Liu:** Supervision (equal); Writing – review & editing (equal). **Hui Tang:** Conceptualization (equal); Funding acquisition (equal); Investigation (equal); Resources (equal); Supervision (equal); Writing – original draft (equal); Writing – review & editing (equal).

DATA AVAILABILITY

The data that support the findings of this study are available from the corresponding author upon reasonable request.

REFERENCES

[1]X. Ma and S. Zhou, "A review of flow-induced vibration energy harvesters," Energy Convers. Manage. **254**, 115223 (2022).

[2]Z. Wen, W. Wang, A. Khelif et al., "A perspective on elastic metastructures for energy harvesting," Appl. Phys. Lett. **120**(2), 020501 (2022).

[3]J. L. Scornec, B. Guiffard, R. Seveno et al., "Self-powered communicating wireless sensor with flexible aeropiezoelectric energy harvester," Renewable Energy **184**, 551–563 (2022).

[4]J. Wang, S. Gu, C. Zhang et al., "Hybrid wind energy scavenging by coupling vortex-induced vibrations and galloping," Energy Convers. Manage. **213**, 112835 (2020).

[5]K. Yang, J. L. Wang, and D. Yurchenko, "A double-beam piezo-magneto-elastic wind energy harvester for improving the galloping-based energy harvesting," Appl. Phys. Lett. **115**(19), 193901 (2019).

[6]X. He, X. Yang, and S. Jiang, "Enhancement of wind energy harvesting by interaction between vortex-induced vibration and galloping," Appl. Phys. Lett. **112**(3), 033901 (2018).

[7]K. Yu, J. J. Liang, B. Y. Qu et al., "Parameters identification of photovoltaic models using an improved JAYA optimization algorithm," Energy Convers. Manage. **150**, 742–753 (2017).

[8]A. Abdelkefi, J. M. Scanlon, E. McDowell et al., "Performance enhancement of piezoelectric energy harvesters from wake galloping," Appl. Phys. Lett. **103**(3), 033903 (2013).

[9]H. Wang, C. Zhao, L. Zeng et al., "Control of the flow around a finite square cylinder with a flexible plate attached at the free end," Phys. Fluids **34**(2), 027109 (2022).

[10]C. Zhao, H. Wang, L. Zeng et al., "Effects of oncoming flow turbulence on the near wake and forces of a 3D square cylinder," J. Wind Eng. Ind. Aerodyn. **214**, 104674 (2021).

[11]F. Ren, C. Wang, and H. Tang, "Active control of vortex-induced vibration of a circular cylinder using machine learning," Phys. Fluids **31**(9), 093601 (2019).

[12]C. Wang, H. Tang, F. Duan et al., "Control of wakes and vortex-induced vibrations of a single circular cylinder using synthetic jets," J. Fluids Struct. **60**, 160–179 (2016).

[13]H. Tang, P. Salunkhe, Y. Zheng et al., "On the use of synthetic jet actuator arrays for active flow separation control," Exp. Therm. Fluid Sci. **57**, 1–10 (2014).

[14]H. F. Wang and Y. Zhou, "The finite-length square cylinder near wake," J. Fluid Mech. **638**, 453–490 (2009).

[15]H. Tang and S. Zhong, "2D numerical study of circular synthetic jets in quiescent flows," Aeronaut. J. **109**(1092), 89–97 (2005).

[16]G. Hu, K. T. Tse, K. C. S. Kwok et al., "Aerodynamic modification to a circular cylinder to enhance the piezoelectric wind energy harvesting," Appl. Phys. Lett. **109**(19), 193902 (2016).

[17]J. Wang, S. Gu, A. Abdelkefi et al., "Enhancing piezoelectric energy harvesting from the flow-induced vibration of a circular cylinder using dual splitters," Smart Mater. Struct. **30**(5), 08LT02 (2021).

[18]G. Hu, K. T. Tse, and K. C. S. Kwok, "Enhanced performance of wind energy harvester by aerodynamic treatment of a square prism," Appl. Phys. Lett. **108**(12), 123901 (2016).

[19]S. Liang, J. Wang, and Z. Hu, "VIV and galloping response of a circular cylinder with rigid detached splitter plates," Ocean Eng. **162**, 176–186 (2018).

[20]T. Zhou, S. F. M. Razali, Z. Hao et al., "On the study of vortex-induced vibration of a cylinder with helical strakes," J. Fluids Struct. **27**(7), 903–917 (2011).

[21]R. Govardhan and C. H. K. Williamson, "Modes of vortex formation and frequency response of a freely vibrating cylinder," J. Fluid Mech. **420**, 85–130 (2000).

[22]C. C. Feng, "The measurement of vortex induced effects in flow past stationary and oscillating circular and D-section cylinders," MSc Thesis, University of British Columbia (1968).

[23]X. Sun, C. S. Suh, Z. Ye et al., "Dynamics of a circular cylinder with an attached splitter plate in laminar flow: A transition from vortex-induced vibration to galloping," Phys. Fluids **32**(2), 027104 (2020).

[24]T. R. Sahu, M. Furquan, and S. Mittal, "Numerical study of flow-induced vibration of a circular cylinder with attached flexible splitter plate at low," J. Fluid Mech. **880**, 551–593 (2019).

[25]G. R. S. Assi and P. W. Bearman, "Transverse galloping of circular cylinders fitted with solid and slotted splitter plates," J. Fluids Struct. **54**, 263–280 (2015).

[26]H. L. Dai, A. Abdelkefi, and L. Wang, "Theoretical modeling and nonlinear analysis of piezoelectric energy harvesting from vortex-induced vibrations," J. Intell. Mater. Syst. Struct. **25**(14), 1861–1874 (2014).

[27]W. Sun, D. Zhao, T. Tan et al., "Low velocity water flow energy harvesting using vortex induced vibration and galloping," Appl. Energy **251**, 113392 (2019).